Polarization of Cinnamoyl-CoA Substrates Bound to Enoyl-CoA Hydratase: Correlation of ^{13}C NMR with Quantum Mechanical Calculations and Calculation of Electronic Strain Energy†

Robert L. D'Ordine,‡,§ Jaroslaw Pawlak,|| Brian J. Bahnson,⊥ and Vernon E. Anderson*,||

Department of Chemistry, Brown University, Providence, Rhode Island 02912, Department of Chemistry and Biochemistry, University of Delaware, Newark, Delaware 19716, and Department of Biochemistry, Case Western Reserve University, Cleveland, Ohio 44106

Received October 9, 2001; Revised Manuscript Received December 7, 2001

ABSTRACT: When α,β-unsaturated substrates bind to the active site of enoyl-CoA hydratase, large spectral changes can be observed [D'Ordine, R. L., et al. (1994) *Biochemistry 33*, 12635−12643]. The differences in the isotropic magnetic shieldings of the free and active site-bound forms of the carbonyl, α-, and β-carbons of the substrates, hexadienoyl-CoA, cinnamoyl-CoA, and (*N*,*N*-dimethyl-*p*-amino)cinnamoyl-CoA have been experimentally determined. The carbonyl and β-carbons are all deshielded, while the α-carbons show increased shielding. These chemical shift perturbations are interpreted to suggest that the π-electrons of the enoyl thiolester are polarized when bound at the active site. Using the crystal structure of (*N*,*N*-dimethyl-*p*-amino)cinnamoyl-CoA bound at the enzyme active site, the shielding tensors were calculated at three different levels of theory, up to a density functional theory model that included all of the contiguous active site residues. These calculations successfully reproduced the observed spectral changes and permitted the electronic polarization of the substrate to be quantified as an electron density difference map. The calculated electron density difference confirms the loss of electrons at the electrophilic β-carbon and carbonyl carbon, while a slight increase in electron density at the α-carbon where proton donation occurs during the hydration reaction and a larger increase in electron density at the carbonyl oxygen are predicted. The energy required to polarize the electrons to the observed extent was calculated to be 3.2 kcal/mol. The force that provides the requisite energy for the polarization is the interaction of the electric field generated by the protein at the enzyme active site with the polarizable electrons of the substrate. Because the induced electronic polarization is along the predicted reaction pathway, the extent of substrate activation by the induced electronic strain is catalytically relevant.

The general principles by which enzymes catalyze chemical reactions have been sought since the original demonstration of cell-free chemical transformations. Even prior to the identification of proteins as the chemical species embodying the catalytic activity of most enzymes, it was proposed that "the act of [interacting with the enzyme] may be accompanied by the intervention of molecular forces which result in a rise in the chemical potential of the reacting substances" (*1*). This concept of strain was given a physical manifestation by the introduction of the "rack mechanism" (*2*), which depicted an enzyme pulling a molecule apart by bond distortion. The original concept of strain embodied an electronic interpretation espoused by Quastel, who noted that "the juxtaposition of certain molecules or groups [generate] locally intense electric fields being a function of the "geography" of [the enzyme]... It is from a consideration of the effects induced in a molecule by the application of an external field that...the mechanism of activation is forthcoming" (*3*).

More recently, the paradigm for enzyme catalysis has focused on transition state stabilization (*4*, *5*). The role of preorganized electrostatic interaction has been promoted by Warshel (*6*−*8*) among others (*9*) to stabilize the transition state. However, even Wolfenden in his seminal contribution (*4*) recognized that, "For catalysis to be observed, the altered substrate must be tightly bound [by the enzyme] in activated forms which approach the transition state." As suggested by Wolfenden and outlined in Scheme 1, ground state destabilization and transition state stabilization are not mutually exclusive. In this paper, we present a general procedure for quantifying how much electronic strain is present in a substrate bound at an enzyme active site by examining the ^{13}C NMR spectra of substrates bound to enoyl-CoA hydratase (ECH).[1]

ECH is a member of the enoyl-CoA isomerase/hydratase superfamily (*10*). The most conserved characteristic of this enzyme superfamily is an active site that binds the CoA thiolester carbonyl via a H-bond to a glycine amide at the

† This work was supported by NIH Grant GM 36562.

* To whom correspondence should be addressed: Department of Biochemistry, Case Western Reserve University, 10900 Euclid Ave., Cleveland, OH 44106-4935. Phone: (216) 368-2599. Fax: (216) 368-3419. E-mail: anderson@biochemistry.cwru.edu.

‡ Brown University.

§ Current address: Monsanto Co., St. Louis, MO 63198.

|| Case Western Reserve University.

⊥ University of Delaware.

10.1021/bi015845h CCC: $22.00
Published on Web 01/30/2002

Scheme 1: Reaction Coordinate Diagram

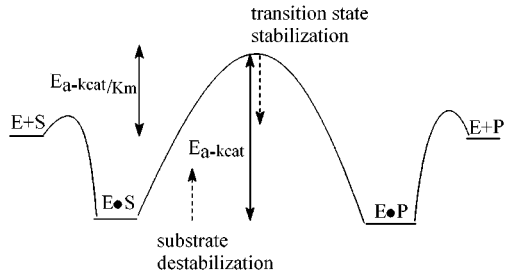

amino terminus of a central α-helix. In ECH, the two amide proton H-bond donors that interact with the thiolester carbonyl are Gly-141 and Ala-68 (*11*, *12*). In this superfamily, these interactions polarize the carbonyl of the thiolester, and consequently stabilize a common enolate or enolate-like transition state which can promote a variety of different chemical reactions (*13*). Mutation of Gly-141 to Pro results in a decrease in k_{cat} of $\sim 10^6$ (*14*).

The electrostatic polarization of the carbonyl thiolesters in enzyme•substrate complexes was characterized initially by large red shifts in the UV spectra of substrates bound to both ECH (*15*) and *p*-chlorobenzoyl-CoA dehalogenase (*16*). When (*N*,*N*-dimethylamino)cinnamoyl-CoA (DAC-CoA) binds to ECH, its λ_{max} is red shifted from 404 to 494 nm (*15*), corresponding to a difference of 13 kcal/mol. This difference in energy can arise from either a destabilization of the bound ground state or a stabilization of the bound electronic excited state. Clearly, if the ground state were to be destabilized by 13 kcal/mol in a manner that favored the reaction, it would provide for a significant catalytic enhancement.

An extensive Raman spectroscopic characterization of the polarization of substrates bound to the dehalogenase has been undertaken (*17*, *18*). These studies have characterized the importance of the amide H-bonds, the α-helix dipole, and the local electric field with respect to the vibrational spectrum of the bound CoA thiolester substrate. These studies qualitatively confirm that there is a detectable electronic rearrangement that occurs in the bound substrate but have not provided a quantitative estimate of the electronic strain.

In this study, the perturbation of the ^{13}C NMR isotropic shieldings of the carbonyl, α-, and *β*-carbons of the enoyl-CoA substrates that occur on binding to the active site of ECH have been measured. We show that the changes in the ^{13}C NMR resonances are consistent with polarization of the enoyl thiolester and that high-level ab initio calculations based on the active site structure of ECH (*55*) successfully predict the observed changes in chemical shifts.[2] The agreement of the observed and calculated ^{13}C NMR spectra permits a quantitative assessment of the extent of electronic polarization present in the bound α,*β*-unsaturated thiolester and its energetic contribution to be made to catalysis.

[1] Abbreviations: Cin-CoA, cinnamoyl-CoA; DAC−CoA, (*N*,*N*-dimethyl-*p*-amino)cinnamoyl-CoA; DFT, density functional theory; DSS, trimethysilylpropanesulfonic acid; ECH, enoyl-CoA hydratase; GIAO, gauge-invariant atomic orbital; HD-CoA, *trans*,*trans*-2,4-hexadienoyl-CoA; SCF, self-consistent field.

[2] The changes in chemical shift and isotropic shielding of a given nuclei are of opposite sign, but identical magnitude; e.g., a decrease in shielding of a ^{13}C nucleus of 2 ppm will result in an increase in the chemical shift of 2 ppm.

MATERIALS AND METHODS

Chemicals. Coenzyme A, lithium salt, was purchased from Sigma Chemical Co. [1-^{13}C,1-^{2}H]Benzaldehyde was from Isotec, Inc. Deuterium oxide (99%), lithium aluminum deuteride ($LiAlD_4$), and sodium [^{13}C]bicarbonate ($NaH^{13}CO_3$) were from Cambridge Isotope Labs. Triethyl phosphono-[1-^{13}C]acetate, triethyl phosphono[2-^{13}C]acetate, benzaldehyde, 4-(*N*,*N*-dimethylamino)benzaldehyde, potassium *tert*-butoxide, *n*-butyllithium (1.6 M solution in hexanes), 4-bromo-*N*,*N*-dimethylaniline, 3-quinuclidinone, and activated manganese(V) dioxide (MnO_2) were from Aldrich Chemical Co.

Enzymes. Beef liver ECH was isolated using a literature procedure (*19*) as modified by Bahnson (*20*). The concentration of the crystalline enzyme was determined by spectroscopic titration with DAC-CoA and an extinction coefficient of 27 800 M^{-1} cm^{-1} at 494 nm for the ECH•DAC-CoA complex (*15*).

Synthesis of CoA Thiolesters. 1-^{13}C- and 2-^{13}C-substituted cinnamic acids were synthesized by the condensation of 1-^{13}C- and 2-^{13}C-substituted TEPA with the appropriate benzaldehyde as previously described (*15*) following a published method (*21*), while [3-^{2}H,3-^{13}C]cinnamic acids were synthesized by condensation of TEPA with the appropriate [1-^{2}H,1-^{13}C]benzaldehyde. The isotopically labeled cinnamic acids were converted to the cinnamoyl imidazoles with carbonyl diimidazole and then to the CoA thiolester following standard procedures (*22*). The CoA thiolesters were purified by reverse phase HPLC as previously described (*15*). [1-^{13}C]Hexadienoyl-CoA and [2-^{2}H,2-^{13}C]hexadienoyl-CoA were synthesized by the condensation of [1,3-$^{13}C_2$]- and [2-^{2}H,2-^{13}C]malonic acid, respectively, with crotonaldehyde as previously described (*23*).

4-(N,N-Dimethylamino)[1-^{13}C,1-^{2}H]benzaldehyde. 4-Bromo-*N*,*N*-dimethylaniline (525 mg, 2.6 mmol) was dissolved in 5−10 mL of freshly distilled THF and cooled to −78 °C. After 15 min, *n*-butyllithium (2.7 mmol) was added dropwise over a 10−15 min period to effect the lithium halogen exchange (*24*). The resultant milky white solution was allowed to stand for 20 min followed by the introduction of $^{13}CO_2$ gas generated from the decomposition of $NaH^{13}CO_3$. A stirred suspension of 500 mg (6.0 mmol) of $NaH^{13}CO_3$ dissolved in THF (1 mL) was reacted with 1 M H_2SO_4 in a sealed 10 mL two-necked round-bottom flask connected, via cannula, to the above reaction mixture. While the cannula was submerged in the reaction mixture, the acid was added dropwise to the $NaH^{13}CO_3$ over a period of 25−30 min until no further evolution of CO_2 was observed. The resultant white acid (*25*) precipitated out of solution, and the reaction mixture was allowed to warm to room temperature. Excess *n*-butyllithium was quenched by the addition of aqueous KOH. The solution was diluted in 100 mL of a $NaOH/H_2O$ mixture (pH 10.0) and extracted with 3 × 50 mL of $CHCl_3$. The pH of the aqueous layer was then adjusted to 4.0, thereby precipitating the acid, which was extracted with 5 × 100 mL of $CHCl_3$. The $CHCl_3$ extract containing the acid was passed through a column of $MgSO_4$ and the solvent removed in vacuo. The recovered 4-(*N*,*N*-dimethylamino)[α-^{13}C]-benzoic acid (334 mg, 2.0 mmol, 77%) was a single spot at the origin of silica gel TLC (90% hexanes and 10% EtOAc) and exhibited a clean ^{1}H NMR spectrum (250 MHz, $CDCl_3$): δ 7.99 (dd, 2H, $^3J_{C-H}$ = 3.0 Hz, J = 9.1 Hz), 6.67

(d, 2H, $J = 8.7$ Hz), 3.06 (s, 6H). IR (CH_2Cl_2) data were consistent with an acid, exhibiting a broad band at 2932 cm^{-1} and a strong band at 1667 cm^{-1}.

4-(*N*,*N*-Dimethylamino)[α-^{13}C]benzoic acid (165 mg, 1.0 mmol) in 10 mL of THF was reduced to the corresponding $^2H_2$-labeled alcohol by addition of $LiAlD_4$ (110 mg, 2.0 equiv) at room temperature and allowed to react for 4 h. Excess $LiAlD_4$ was quenched by the addition of wet THF, and aluminum oxides were removed by filtration through a short stack of $MgSO_4$. The solvent was removed by rotary evaporation and the residue dried in vacuo. The recovered alcohol (150 mg, 0.97 mmol, 97%) was a clear oil which gave a single TLC spot (50% hexanes/EtOAc) and exhibited a clean ^{1}H NMR spectrum (250 MHz, $CDCl_3$): δ 7.23 (dd, 2H, $^3J_{C-H} = 4.3$ Hz, $J = 8.8$ Hz), 6.73 (d, 2H, $J = 7.5$ Hz), 2.93 (s, 6H). The resonance for benzylic protons at 4.49 ppm, in comparison to that of the nonlabeled alcohol, was <5% due to ^{2}H replacement. IR (CH_2Cl_2): 3381 cm^{-1} (no carbonyl band observed).

4-(*N*,*N*-Dimethylamino)[α-^{13}C,α-$^2H_2$]benzyl alcohol (150 mg, 0.97 mmol) was oxidized to the aldehyde by reaction with 20 equiv of MnO_2 (*26*) in 20 mL of THF for 4−6 h. TLC (75% hexanes and 25% EtOAc) showed numerous spots, including the aldehyde as compared to authentic material. The yields for a single oxidation were poor, necessitating the recycling of recovered starting materials. After each oxidation, the aldehyde, alcohol, and yellow and orange contaminants were separated by flash chromatography (*27*) on a 300 mm × 20 mm silica gel column with a solvent system of 75% hexanes and 25% EtOAc. Recovered alcohol was recycled. 4-(*N*,*N*-Dimethylamino)[α-^{13}C,α-^{2}H]benzaldehyde (80 mg) crystallized as white plates with a slight yellow tint. The R_f, 0.3 (75% hexanes and 25% EtOAc on silica gel TLC), of the product aldehyde was identical to that of an authentic sample. The ^{1}H NMR data (400 MHz, $CDCl_3$) [δ 7.75 (dd, $^3J_{C-H} = 4.6$ Hz, $J = 9.0$ Hz, 2H), 6.70 (d, 2H, $J = 8.8$ Hz), 3.09 (s, 6H)] matched those of the authentic sample with the exception that the aldehyde resonance at 9.75 ppm was not observed, confirming the deuteration of the aldehyde proton.

Triethyl Phosphono[2-^{13}C,2-$^2H_2$]acetate. Triethyl phosphono[2-^{13}C]acetate was converted to triethyl phosphono[2-^{13}C,2-$^2H_2$]acetate by incubation with 0.35 M 3-quinuclidinone in D_2O (pD 8.1) for 48 h. The exchange solution was acidified to pD 1.0−2.0 with 1 M HCl and triethyl phosphono[2-^{13}C,2-$^2H_2$]acetate extracted with 4 equal volumes of $CHCl_3$. The pooled extracts were washed with 0.1 N HCl and dried with $MgSO_4$, and the solvent was removed by evaporation. ^{1}H NMR data ($CDCl_3$) indicated there was 97% incorporation of ^{2}H at C-2.

^{1}H NMR Spectroscopy. All ^{1}H NMR spectra of the CoA thiolesters were acquired on a Bruker AM 400 MHz NMR spectrometer in D_2O. ^{1}H NMR spectra of other materials were acquired in solvents as noted on either a Bruker AM 400 MHz or WM 250 MHz spectrometer. The probe temperature was always 24−26 °C. Chemical shifts for the CoA thiolesters are reported with respect to external trimethysilylpropanesulfonic acid (DSS). The internal chemical shift standard, for the CoA thiolesters, was the triplet at 2.43 ppm due to protons (t, 2H) on C-6″ of the pantetheine backbone (*28*).

Preparation of ECH for ^{13}C NMR Experiments. A 5 mL crystalline sample of ECH (∼5−6 mg/mL) stored at −20 °C was thawed at 4 °C. The crystals were collected by centrifugation. The crystalline ECH was resuspended in 100−200 μL of filtered (0.22 μm cellulose acetate Costar mini filters) 100 mM potassium phosphate (pD 7.85 ± 0.1) in D_2O and transferred to an Eppendorf centrifuge tube. The suspension of ECH was then placed in a centrifugal vacuum evaporator for 1 h to remove residual ethanol. The protein sample was dissolved in 450 ± 25 μL of the same buffer and gently mixed at room temperature for 1 h. The solubilized protein sample was then centrifuged at 12000*g* for 5.0 min to clear the solution of any denatured protein. The active ECH concentration was determined by using the extinction coefficient of the DAC-CoA·ECH complex of 27 800 M^{-1} cm^{-1} at 494 nm. The concentration of active sites for all NMR experiments was between 2.0 and 2.5 mM. The pD (7.8 ± 0.3) and temperature of solubilization (15−30 °C) are crucial factors in the preparation of clear, concentrated samples of ECH. Addition of substrate significantly improves solubilization of the enzyme. The pD of the samples was checked before and after experiments and was always 7.8 ± 0.3. The active ECH concentration determined at the end of the experiment was at least 80% of that determined at the start. All samples contained trace amounts of ethanol and EDTA retained from the crystalline suspensions.

^{13}C NMR of ECH·α,β-Enoyl-CoA Complexes. The ^{13}C NMR spectra of the ECH·cinnamoyl-CoA complexes were obtained in 5 mm NMR tubes using a Bruker AM 400 MHz NMR instrument operating at 100.61 MHz. All spectra of ECH·CoA complexes, consisting of 20000−26000 transients, were acquired with broad band ^{1}H decoupling (decoupler power of 0.5 W), pulse widths of 45 μs, recycle delays of 2.0 s, at 26 ± 1 °C, and a spin rate of 17 rps. Spectra of uncomplexed ECH were acquired prior to the addition of the substrate to ECH. Spectra of uncomplexed substrates were acquired independently. Concentrated stock substrate solutions were used for addition to the ECH samples to minimize dilution. Substrate, equal to approximately 0.75 equiv of ECH active sites, was added first, and then successive titrations were performed to observe both bound and free species. The ^{13}C NMR experimental conditions used in these studies were adapted from those described in ref *29* for acquiring ^{13}C NMR spectra of labeled substrates when bound to porphobilinogen synthase, an enzyme with an M_r of 280 kDa.

Construction of the Bovine ECH Active Site Model. The crystal structure of DAC-CoA bound at the active site of recombinant rat liver ECH [PDB entry 1EY3 (*55*)] provided the initial coordinates for this structure. The model developed for calculating the ^{13}C shielding of the bound CoA and catalytic water included every amino acid within a 5 Å radius of the carbon−carbon double bond of the α,β-unsaturated thiolester. The N-terminal ends of amino acid residues were capped by formyl groups [−HNC(═O)H], and the C-terminal ends were capped as amides (−$CONH_2$). The active site contained 10 amino acids conserved between rat and bovine enzymes: Ala-98, Met-103, Leu-117, Trp-120, Gly-141, Glu-144, Glu-164, Gly-172, Ala-173, and Phe-263. The conservation of all active site residues between rat and bovine ECH

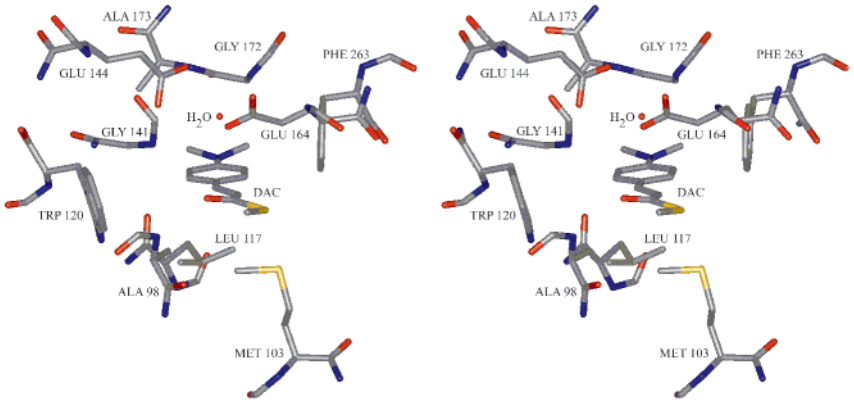

FIGURE 1: Stereoscopic view of the DAC-CoA·ECH active site used for ^{13}C NMR calculations. To improve the quantum chemical NMR calculations, the active site of ECH was optimized using the ONIOM method. The key residues are labeled. The amides of Gly-141 and Ala-98 interact favorably with the thiolester carbonyl, and Glu-144 and Glu-164 both H-bond to the substrate water molecule directly above the double bond between C-2 and C-3 that would be hydrated during the catalytic reaction.

allowed us to develop a working bovine ECH active site model (*67*). The carboxylate of Glu-144 was deprotonated. To determine if the protonation state of Glu-164 affects the spectroscopic properties of the bound substrate, two models of the active site were considered: one where Glu-164 is protonated (DAC-1) and a second where Glu-164 is unprotonated (DAC-2). The DAC-CoA was truncated to the *S*-methyl thiolester. This structure of the ECH active site is shown in Figure 1.

Calculation of NMR Shielding Parameters. De Dios and Oldfield introduced a charge field approach to calculating NMR shielding constants. The NMR shielding of a nucleus was dissected into short- and long-range electronic effects, while other intramolecular shielding arising from ring current and susceptibility effects was determined to be minimal for heavy atoms (*30*, *31*). They, and others (*32*, *33*), have implemented methods for calculating NMR properties of large systems where the short-range electronic effects are determined by high-level ab initio calculations and the long-range electrostatic effects are included at lower levels of theory. We have implemented this conceptual approach to calculate the change in shielding parameters observed when ligands bind to the ECH active site. The shielding parameters for the α,β-unsaturated thiolesters were obtained using the gauge-invariant atomic orbital (GIAO) method (*34*, *35*) with three different electronic representations of the optimized active site. All calculations began with the ONIOM-optimized active site geometry (*36*), implemented in Gaussian 98 (*37*). In this procedure, the molecular system being studied is divided into two layers, which are treated with different levels of theory. The reactants, including the 4-(dimethylamino)cinnamoyl thiolester and molecule of water, were treated with density functional theory (DFT) at the B3LYP/6-31G(d) level (*38*), whereas the model of the enzyme active site was treated at the PM3 level of theory. The virtue of this procedure is that the interactions between the ligand and active site are evaluated at a defined level of theory (in this case using PM3), while the electronic distribution within the ligand is determined at a sufficiently high level to permit accurate calculation of the NMR properties (*32*). During optimization, the positions of the atoms of the peptide backbone were frozen at their crystallographic positions. The optimization of geometry was terminated when the entire system reached the default Gaussian convergence criteria for forces.

Following the charge field approach (*30*), the atoms of the active site amino acids were replaced with partial charges. A Mulliken population analysis from a single-point calculation where every atom of the system was treated at the B3LYP/6-31G(d) level of theory was undertaken to obtain an effective partial charge distribution. The shielding constants for the substrate water and thiolester were then calculated at the B3LYP/6-31G(d) level in the presence of this charge field.

Using the ability of the ONIOM method to evaluate the electronic contributions at different levels of theory, a GIAO calculation with the active site amino acids modeled at the PM3 level while the substrate water and thiolester were modeled at the B3LYP/6-31G(d) level was performed. In this calculation, the chemical shift calculation was performed using the same basis sets that were used in the geometry optimization. Finally, the GIAO shielding constants were computed for the entire active site in the −2 state at the B3LYP/6-31+G(d,p) level using the facilities of the Ohio Supercomputer Center (~400 CPU hours).

Calculation of the Active Site Electric Field. The contribution to the electric field at the active site of residues not included explicitly in the ECH active site model was evaluated using DelPhi (*39*) with the atomic charges taken from AMBER 4.0 (*40*). The partial charges on the atoms included explicitly in the active site model were taken from the Mulliken charge analysis. The charges on the DAC-CoA atoms were set to 0, except for the nonbridging phosphate oxygens which were charged to represent the fully ionized forms.[3] ECH is a hexamer composed of two trimers. The trimer is required for activity as the extended active sites are comprised by contributions from two subunits. To evaluate the active site electric fields using DelPhi, the trimer composed of the first three subunits in 1EY3 was analyzed.

Electron Density Difference Map. The polarization of DAC-CoA induced by binding to the ECH active site was visualized by determining the difference in electron densities

[3] The charges on the DAC-CoA thiolester were omitted because the question to be answered is, "What is the electric field at the active site generated *by the enzyme*?"

between the ECH·DAC-CoA complex and the uncomplexed enzyme and ligand (eq 1).

$$\Delta\mathcal{E} = \mathcal{E}_{\text{ECH·DAC-CoA}} - \mathcal{E}_{\text{ECH}} - \mathcal{E}_{\text{DAC-CoA}} \qquad (1)$$

$\mathcal{E}$ represents the identically sized electron density cube files for the subscript molecule(s). $\mathcal{E}$ for ECH and DAC-CoA was maintained at the same size by converting the other molecule to dummy atoms and using the NOSYMM keyword. All calculations were performed at the B3LYP/6-31G(d) level. The electron difference cube file, $\Delta\mathcal{E}$, was visualized using the program gOpenMol (*41*−*43*, *66*).

Electronic Strain Calculation. The optimized ONIOM active site model was used as the basis structure for the calculation of the electronic strain energy. The strain was calculated by determining the self-consistent field (SCF) electron density at the B3LYP/6-31G(d) level in the presence of each protein atom being represented by the Mulliken point charge determined from the active site model. This electron density was saved in the checkpoint file, and then the active site point charges were set to zero in the job definition file. The energy of the electronic system was then determined for every iteration of the SCF calculation by using the #P and Guess=Read options in Gaussian 98. The electronic polarization energy is the difference between the energy of the system with the restored electron density and the final SCF energy.

RESULTS

^{13}C NMR of ECH·α,β-Enoyl Thiolester Complexes. ECH is a 168 kDa homohexamer of ∼28 kDa monomers (*44*, *45*). The large size of the complex broadens the observed ^{13}C resonances of bound substrates. The crystal structure of bound DAC-CoA indicates that the α,β-thiolester is tightly bound in the interior of the protein, with little disorder that would provide a more anisotropic environment. Due to the tumbling correlation and relaxation times associated with large proteins (*46*), the ^{13}C NMR line width of the substrate bound in the active site of ECH is anticipated to be very broad. With this in mind, all of the methine protons in the α,β-unsaturated CoAs were synthesized with ^{2}H present on the labeled carbon to minimize the ^{13}C−^{1}H dipolar relaxation, the dominant mechanism of relaxation at these molecular masses and tumbling correlation times, and thus minimize the line width. As shown in Figure 2, it was then possible to observe the ^{13}C resonances for the β-^{13}C of DAC-CoA. The background ^{13}C resonances from the protein do not obscure the regions of interest for this study. The titration of the active sites permitted both the free and bound ^{13}C resonances of the α,β-unsaturated substrates to be identified. The ECH spectrum, including amide carbonyls resonances from 165 to 185 ppm, aromatic carbon resonances from 125 to 130 ppm, and aliphatic carbon resonances from 10 to 70 ppm, displayed no detectable changes on binding of DAC-CoA.

Figure 3 shows expansions of the ^{13}C NMR spectrum for the carbonyl, α-, and β-carbons of DAC-CoA. The ^{13}C resonances of unbound DAC-CoA appear at 195.7, 121.7, and 144.9 ppm, respectively, in spectral windows that are not complicated by protein ^{13}C resonances. When DAC-CoA binds to ECH, two additional resonances are apparent for each ^{13}C-labeled carbon. These data are listed in Table 1.

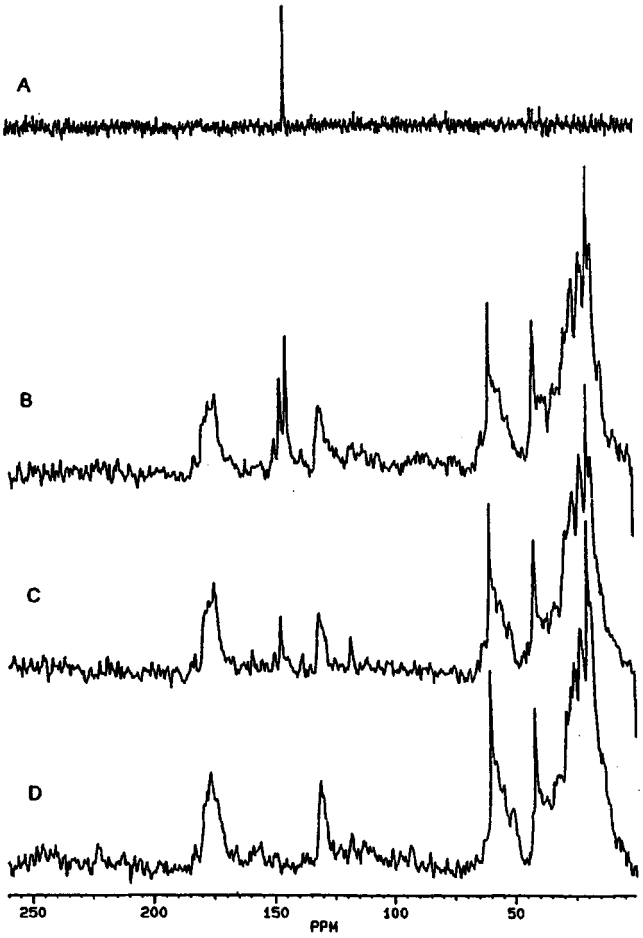

FIGURE 2: ^{13}C NMR spectra (100.6 MHz) of ECH and [3-^{13}C,3-^{2}H]DAC-CoA. Full spectral width shown (0−260 ppm). (A) Free [3-^{13}C,3-^{2}H]DAC-CoA, 6.0 mM, NS = 460, LB = 10 Hz. (B) Bound and free [3-^{13}C,3-^{2}H]DAC-CoA, 1.3 DAC-CoA/ECH ratio. (C) Bound [3-^{13}C,3-^{2}H]DAC-CoA, 0.7 DAC-CoA/ECH ratio. (D) Spectrum of 2.1 mM ECH. Note the aliphatic region of the protein between 10 and 50 ppm, the aromatic/unsaturated region at 125−135 ppm, and the amide/carbonyl region at 170−185 ppm. (B−D) NS = 25−28000, processed with LB = 25 Hz.

The appearance of two different perturbed resonances for DAC-CoA suggests that there are two different populations of bound DAC-CoA that interconvert at less than ∼500 s^{-1}. The presence of two bound species has been suggested by stopped-flow studies where a transient intermediate with a smaller red shift is observed that converts to the more UV-polarized species with a rate constant of <100 s^{-1} (V. E. Anderson and co-workers, unpublished observations). It is possible that these separate resonances arise from two different conformations, but another intriguing possibility is that they arise from different protonation states of the active site.

Similar spectra were acquired for C-1, C-2, and C-3 of Cin-CoA as well as C-1 and C-2 of HD-CoA. These substrates do not bind as tightly to ECH, and consequently, the free and bound substrates were in a slow exchange regime, resulting in a broadened average peak being observed rather than the individual resonances for the free and bound species. Since the experiments with excess enzyme were conducted at 1−2 mM enzyme, a concentration at least 10-fold greater than the K_ds of 50−100 μM for these substrates, the ^{13}C resonance of the initial spectrum with ECH in 25% excess is characteristic of the bound substrate. The magni-

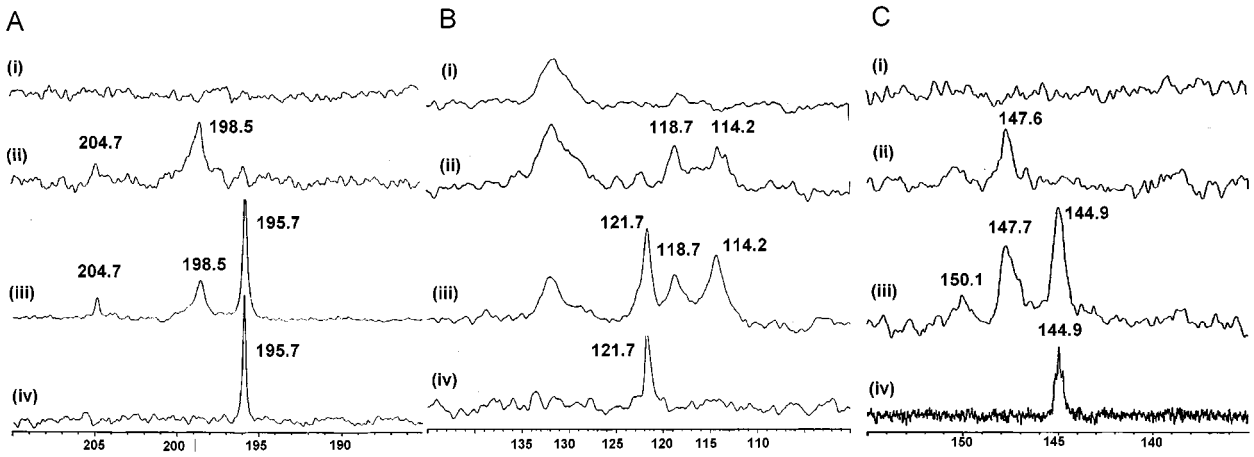

FIGURE 3: ^{13}C NMR spectra (100.6 MHz) of ECH and ^{13}C-substituted DAC-CoAs. (A) [1-^{13}C]DAC-CoA: (i) 1.9 mM ECH, (ii) [1-^{13}C]-DAC-CoA·ECH complex with a 0.90 [1-^{13}C]DAC-CoA/ECH ratio, (iii) excess [1-^{13}C]DAC-CoA with a 1.6 DAC-CoA/ECH ratio, and (iv) free [1-^{13}C]DAC-CoA (5.2 mM). (B) [2-^{13}C,2-^{2}H]DAC-CoA: (i) aromatic region of ECH (2.2 mM) and (ii−iv) same as described for panel A. (C) [3-^{13}C,3-^{2}H]DAC-CoA: (i−iv) same as described for panel A.

Table 1: ^{13}C NMR Chemical Shifts (ppm) Observed for Labeled α,β-Unsaturated Substrates

	1-^{13}C[a]			2-^{13}C,2-^{2}H[b]			3-^{13}C,3-^{2}H[c]		
CoA	free	bound	shift	free	bound	shift	free	bound	shift
Cin-CoA	195.9	201.0	5.1	126.9	126.1	−0.8	144.0	147.2	3.2
DAC-CoA[d] (1)	195.7	198.5	2.8	121.7	118.7	−3.0	144.9	147.7	2.8
DAC-CoA[d] (2)		204.7	9.0		114.2	−7.5		150.1	5.2
HD-CoA	196.5	200.8	4.3	127.7	124.8	−2.9			

[a] The extent of ^{13}C labeling was ≥98% in all species. [b] The percentage of deuterium label on C-2, as determined by integration of residual protons in the NMR, was as follows: 70% for HD-CoA, 50% for DAC-CoA, and 30% for Cin-CoA. [c] The percentage of deuterium label on C-3 was as follows: >95% for DAC-CoA and >98% for Cin-CoA. [d] The ^{13}C NMR spectra of DAC-CoA were typified by two new resonances as shown in Figure 3.

tudes of the observed changes in chemical shift are similar to those observed for the less perturbed form of DAC-CoA and are included in Table 1. Qualitatively, the chemical shifts for all of the carbonyl carbons (C-1) are deshielded in the enzyme complex, while all of the C-2 atoms were more shielded and the C-3 atoms deshielded. To the extent that the differences in shielding reflect changes in π-electron density (vida infra), these changes in chemical shift are consistent with a polarization of both the carbonyl and α,β-carbon double bond of these enoyl thiolester substrates when bound at the active site of ECH.

The identification of the perturbed ^{13}C resonances as arising from the ECH·DAC-CoA complex was confirmed by the addition of unlabeled DAC-CoA. This addition resulted in an increase in the intensity of the resonances of the free species and a loss of both resonances attributed to bound species. The ability of unlabeled DAC-CoA to displace the ^{13}C-labeled material from the active site indicates that the resonances from the bound DAC-CoA are due to reversibly bound complexes.

The widths of the ^{13}C resonance from the uncomplexed thiolester in the presence of the bound species are given in each figure legend. Figure 3B shows the results of this experiment with [2-^{13}C]DAC-CoA. The resonance for the uncomplexed species at 121.7 ppm is broadened by 51 Hz in comparison to the line width in the absence of the enzyme. The line broadening of the signal arising from the free DAC-CoA is due to the chemical exchange between the complexed and uncomplexed forms of DAC-CoA. The rate constant for dissociation of DAC-CoA from the ECH complex can be determined according to eq 2, where obsd refers to the line width in the presence of the enzyme and free in the absence (*47*).

$$\pi\Delta\nu_{1/2,\mathrm{obsd}} = \pi\Delta\nu_{1/2,\mathrm{free}} + k_{-1} \qquad (2)$$

The 51 Hz broadening observed for the unbound [1-^{13}C]-DAC-CoA yields an apparent dissociation rate constant of 160 s^{-1}; since DAC-CoA has a kinetically determined K_D of 1.8 μM, this implies that the association rate constant is 8.9×10^7 M^{-1} s^{-1} under these conditions. It should be noted that it is assumed that exchange is the only factor in the difference in the broadness of the free resonances. These numbers are regarded as upper and lower limits for the dissociation and association rate constants, respectively.

For the other α,β-unsaturated CoA thiolesters in this study, the presence of both free and bound substrate resulted in a broad resonance at an intermediate chemical shift, characteristic of the intermediate chemical exchange regime where the rate constant for exchange is comparable to the difference in chemical shift (*48*), as shown in eq 3 where $\Delta\nu$ is the separation, in hertz, between the two species in question.

$$k_{\mathrm{ex}} = (\pi/\sqrt{2})\Delta\nu \qquad (3)$$

Calculation of Anisotropic Shielding Parameters. The active site of the ECH·DAC-CoA complex was optimized in a mixed mode calculation so that the geometry of the bound ligand would be consistent with the level of theory used to calculate the spectroscopic parameters. This optimization resulted in very minor changes in the active site.

Table 2: Calculated Anisotropic Shielding Constants for *S*-Methyl(*N*,*N*-dimethyl-*p*-amino)thiocinnamic Acid[a]

		ONIOM[b]		net charge[c]	
atom	unbound DAC	DAC-2[d]	DAC-1[e]	DAC-2[d]	DAC-1[e]
O-4	−131.5	−163.3	−167.6	−140.1	−117.0
C-1	10.7	6.5	6.6	0.4	2.0
C-2	78.3	79.6	80.4	68.5	79.2
C-3	54.3	51.0	53.1	45.8	50.6
S-5	382.6	369.5	366.9	677.0	438.8
C-8	73.3	70.3	71.8	9.7	53.0
C-9	69.1	67.3	67.3	67.2	66.8
C-10	84.0	82.4	83.5	68.8	76.6
C-11	49.3	47.3	48.9	7.3	28.2
C-12	84.8	83.9	85.1	73.2	79.0
C-13	60.0	60.6	60.1	61.4	59.5
N-18	196.1	194.5	193.6	185.3	170.4
C-19	149.7	149.2	149.5	192.7	172.8
C-20	149.6	149.3	149.8	195.8	179.6
N-27	176.2	172.3	172.4	206.2	184.1

[a] Truncated theoretical model of DAC-CoA. [b] Shielding constants calculated by the GIAO method for the ONIOM model of the ECH complex. [c] Shielding constants calculated by the GIAO method using partial charges to represent active site atoms. [d] Glu-164 is unprotonated, with an overall active site charge of −2. [e] Glu-164 was protonated, with an overall active site charge of −1.

One surprising characteristic of the 1EY3 crystal structure was that the cinnamoyl thiolester was not planar, and the torsion angle between C-3 and the aromatic ring,varied between 12° and 29° in the six active sites of the ECH hexamer (*55*). The ONIOM-optimized structure retained this nonplanarity with the torsion angle being 12.1°, while in the gas phase calculation, the conjugated system is planar. The ONIOM method has been used to calculate shielding constants for larger molecules (*32*). The calculated anisotropic shielding parameters for the unbound and bound (*N*,*N*-dimethyl-*p*-amino)cinnamoyl thiolester are presented in Table 2. The important result in Table 2 is that the observed differences in shielding for C-1, C-2, and C-3 match that observed experimentally both in sign and in magnitude (Table 1).

Two other significant observations are contained in Table 2. The calculation of the ^{13}C shielding constants was largely independent of whether Glu-164 was protonated or unprotonated. While, we initially anticipated that the increased negative charge in the unprotonated (−2) form would enhance the polarization of the conjugated enoyl-thiolester, the position of the charge directly above the π-system only results in a large change in the local electric field orthogonal to the π-system, which has a minimal effect on the calculated shielding constants. The second important observation is that using point charges derived from the quantum chemical calculation was not an effective procedure to predict the experimentally observed shielding constants and yielded physically unrealistic results (e.g. shielding parameters for C19 and C20).

Electric Field at the Active Site. DelPhi calculations (*39*) were undertaken to determine the electric field at the ECH active site. These calculations determine the contributions of all charges and the effect of the solvent dielectric on the electric field at any given point. Including the atoms of DAC-CoA as dummy atoms in the calculation permitted a determination of both the electrostatic potential and the

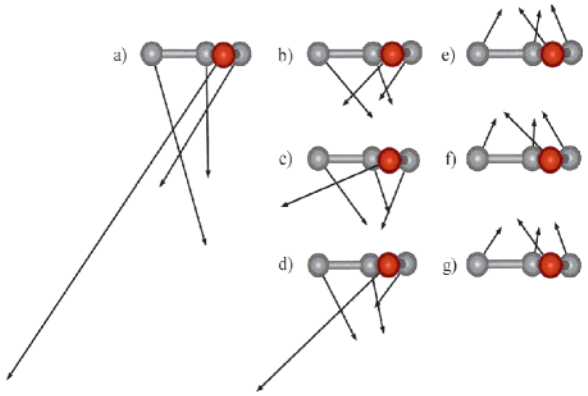

FIGURE 4: Electric field vectors at ECH active sites. The enoyl thiolester is placed in the $x-z$ plane and is oriented so that the α,β carbon−carbon double bond is along the x-axis. The electric field vectors give the magnitude and direction of the electrostatic force at the four nuclei of the conjugated π-system. The electric field has been calculated using DelPhi (*39*) for our active site model in panel a. It is clear that the electric field varies in both magnitude and direction across the enoyl thiolester. The electric field of the model is comparable to the electric field at three different active sites of the first three subunits that form a trimer of the 1EY3 ECH structure (b−d). The electric fields shown in structures e and f are the corresponding electric fields that result from the residues omitted from the quantum mechanical model. These structures indicate that the omitted residues will contribute a modest increase to the polarization of the enoyl thiolester, but that it is a modest fraction of the total electric field.

electrostatic potential gradient (electric field) at each of the atoms of the substrate enoyl thiolester. The contribution from any particular feature can be dissected by setting all other charges to zero. The results for the calculation of the electric field at each atom of the DAC-bound thiolester from only the atoms included in the quantum chemical model are depicted in Figure 4a. The electric fields determined by including all of the protein at the three different active sites of the catalytic trimer using AMBER charges for the protein residues are shown in Figure 4b−d. The qualitative conclusion from these calculations is that the electric field from the residues included in the quantum chemical model accurately reflects the electric field present at the active site. It follows that additional contributions from the extension of the α-helix or other residues would not significantly alter the electrostatic properties of the active site.

A second important observation is that there is a significant variation of both the magnitude and direction of the electric field vectors across the enoyl system. These variations indicate that the electric field is a strong function of atomic position and that changes in position of less than 1 Å will result in significantly different electrostatic interactions. The strong dependence of the electric field on position may also be responsible for the differences in the electric fields determined at each of the three active sites with three different positionings of the substrate.

Magnitude of Electronic Polarization. The calculated electronic polarization induced in DAC-CoA by binding at the active site is shown in Figure 5. This figure emphasizes that the greatest electronic polarization occurred along the carbonyl and carbon−carbon double bonds. The results show that there was a loss of electron density at C-3 and the carbonyl carbon while there were increases in electronic density on the carbonyl oxygen and, to a lesser extent, on

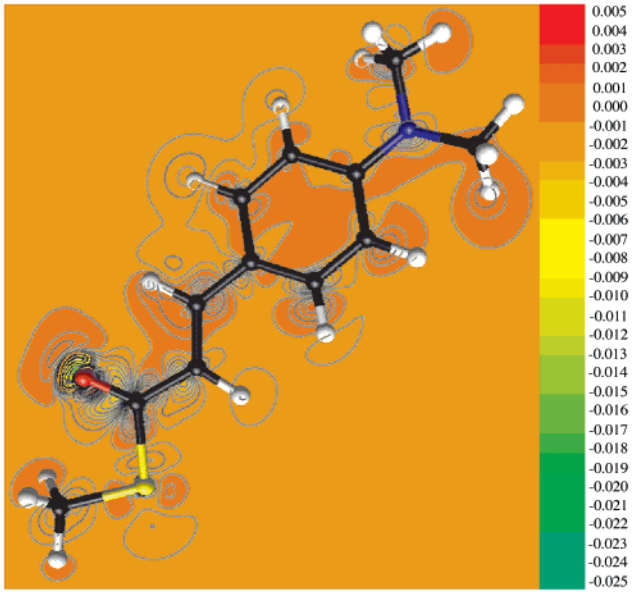

FIGURE 5: Electron density difference map of the ECH·DAC-CoA complex. The electron density difference map that represents the electronic polarization of the substrate and enzyme active site is superimposed on the DAC·thiolester coordinates. The color scheme key is given at right with the units being electrons per cubic angstrom. The contour lines are drawn at 0.001 electron/Å^3. The key feature of this figure is the fact that the electronic polarization is focused on the α,β-unconjugated π-system of the substrate that is activated for nucleophilic addition at the β-carbon.

C-2. The system was too large for an NBO analysis using Gaussian 98, so only the Mulliken analysis of assigning electrons to specific atoms was investigated. Table 3 reports the Mulliken charge analysis of the electronic distribution from the −1 and −2 protonation state models. Qualitatively, the results for the −2 model show changes consistent with those represented in Figure 5. Quantitatively, the magnitude of the electronic rearrangement is 0.02−0.05 electron, i.e., <1/20 of an electron. This magnitude of electronic rearrangement is consistent with the experimentally observed changes in chemical shielding where a 5 ppm change in shielding would correspond to a decrease in electron density of 0.03 e according to the Speisecke−Schneider rule of 160 ppm/π-electron (*49*).

Electronic Strain Energy. The electronic strain energy was determined from the difference in energy of the electronic distribution present at the active site minus the optimized SCF electronic energy for the same conformation of the ligand in the absence of the active site electric field. The rationale for this definition is presented in the Discussion. For DAC-CoA bound to the −2 model of the ECH active site, the electronic strain energy calculated at the B3LYP/6-31+G(d) level is 3.2 kcal/mol. As explored further in the Discussion, this value is an estimate based on the restrictions of the model. There is a minimal dependence on the assumption of the protonation state, as protonating Glu-164 only modestly changes the electric field in the plane of the enoyl system. A dielectric constant of unity was appropriately employed since the calculation involved a potential rearrangement and polarization of the interacting atoms; however, this could lead to an overestimate. The truncation of the active site and the strict definition of polarization energy suggest that 3.2 kcal/mol is more probably a lower estimate.

Table 3: Charge Distribution Obtained by a Mulliken Population Analysis of *S*-Methyl(*N*,*N*-dimethyl-*p*-amino)thiocinnamic Acid[a] Unbound and in a Complex with ECH

atom	DAC uncomplexed	DAC-2[b]	DAC-1[c]
O-4	−0.460	−0.500	−0.511
C-1	0.255	0.289	0.245
C-2	−0.197	−0.217	−0.227
C-3	−0.155	−0.136	−0.178
S-5	0.084	0.107	0.108
H-6	0.145	0.153	0.157
H-7	0.163	0.166	0.170
C-8	0.174	0.199	0.194
C-9	−0.185	−0.171	−0.170
C-10	−0.192	−0.219	−0.193
C-11	0.376	0.381	0.396
C-12	−0.196	−0.217	−0.217
C-13	−0.200	−0.204	−0.196
H-14	0.135	0.146	0.135
H-15	0.131	0.132	0.144
H-16	0.137	0.159	0.160
H-17	0.130	0.142	0.155
N-18	−0.472	−0.472	−0.471
C-19	−0.315	−0.317	−0.326
C-20	−0.315	−0.331	−0.341
H-21	0.166	0.146	0.159
H-22	0.163	0.179	0.181
H-23	0.160	0.143	0.154
H-24	0.160	0.141	0.152
H-25	0.163	0.185	0.195
H-26	0.164	0.179	0.192
C-27	−0.611	−0.596	−0.589
H-28	0.183	0.168	0.186
H-29	0.183	0.266	0.196
H-30	0.240	0.198	0.218

[a] Truncated theoretical model of DAC-CoA. [b] Glu-164 is unprotonated, with an overall active site charge of −2. [c] Glu-164 was protonated, with an overall active site charge of −1.

DISCUSSION

When α,β-unsaturated substrates bind at the active site of ECH, it is clear that their spectroscopic properties are significantly altered. Previous investigations characterized the change in the UV absorbance of para-substituted cinnamoyl-CoAs (*15*). The systematic variation of UV absorbance together with the significant red shifts of the enoyl thiolester stretching vibrations observed in the Raman vibrational spectra (*50*) and the changes in the ^{13}C NMR shielding constants have now confirmed that the electronic distribution of the ground state is perturbed upon binding. However, in the UV spectra, the red shift of the λ_{max} was a strong function of the para substituent (*15*), while the effects of the electronic polarization of HD-CoA, Cin-CoA, and DAC-CoA observed in the ^{13}C NMR spectra were all of similar magnitude.

There are three different effects that can cause an alteration of the spectral properties of a ligand on binding. The first is a change in conformation. For carbon, rotation about σ-bonds can produce significant alterations in shielding. This effect is responsible for the observed correlation between secondary structure and the ^{13}C chemical shift for C_α in proteins (*51*, *52*). The restriction of a bound ligand to a single conformation can result in both a sharpening of spectral features and a shift in position as observed by Raman spectroscopy (*53*). In the case of α,β-unsaturated CoA thiolesters binding to ECH, experimental evidence indicates this contribution will

be minimal. The bound conformations of HD-CoA and of DAC-CoA have been characterized by NMR (*54*) and crystallography (*55*). The most important torsion angle, because it orients the reactive double bond between C_α and C_β relative to the carbonyl, is the O═C−C═C torsion angle of 0°, indicating the thiolester is in an *s-cis* conformation (*56*). This *s-cis* conformation is the predominant solution structure for α,*β*-unsaturated thiolesters (*57*). The thiolester torsion angles of the bound CoAs (C−S−C−O) are near 0°, which is common for most thiolesters (*57*). Thus, the bound conformations of the CoA thiolesters in this study are characteristic of the predominant solution structures, making it difficult to ascribe the observed changes in ^{13}C NMR spectra to changes in conformation.

The second perturbation of ^{13}C NMR shielding constants can come from ring current effects and other intermolecular magnetic susceptibility contributions. The structures of the ECH active site and of the bound DAC-CoA indicate that there are no *π*-electrons within 4 Å of the enoyl thiolester C atoms, ruling out the possibility of ring current effects generating the observed changes. The third effect that can cause changes in the ^{13}C shielding parameters is the electrostatic environment of the active site, which includes both the close intermolecular interactions of the H-bonds from Gly-141 and Phe-98 and the more distant interactions of the active site carboxylates of Glu-144 and Glu-164 and the α-helical dipole of residues 141−148. The contributions of these interactions were examined at three different levels of theory: using assigned partial charges at the nuclear positions, at the PM3 level using an ONIOM calculation, and at the DFT level.

When substrates bind at an enzyme active site, they become conformationally constrained by specific interactions with active site functional groups. Crystal structures of many enzyme·substrate and enzyme·inhibitor complexes have confirmed these interactions. The well-defined electron density in the crystal structures can clearly identify the conformation of the ligand and the relative orientation of the interacting groups. However, the strength of these interactions and their roles in catalysis are less well identified by the crystal structure.

Here we provide a conceptual process for determining the extent of electronic polarization and consequently for quantifying the resulting electronic strain. These questions are inherently of a quantum chemical nature since they require the determination of the distribution of electrons and the energetic evaluation of the distribution. This process is outlined in Scheme 2.

In Scheme 2, the solution structure of the substrate enoyl thiolester is shown as A. When the structure binds to the enzyme, the conformation, including bond lengths and angles, is perturbed slightly as determined by the ONIOM calculation. The validity of the computational model was supported by its ability to reproduce the crystallographically observed nonplanarity of the α,*β*-double bond with the phenyl ring. From this structure, the electronic polarization due to the electrostatic interactions with the active site was determined by replacing the protein atoms with the Mulliken point charges determined in the ONIOM calculation[4] (structure B in Scheme 2). Thus, the SCF electronic distribution of the substrate in the presence of these point charges is determined and saved. The point charges are set to 0

Scheme 2: Calculation of Electronic Strain

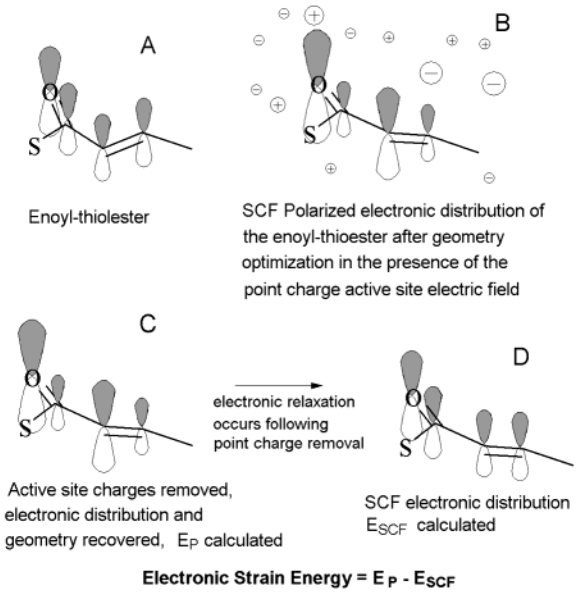

(structure C), and the saved electron density is retrieved. Since structures B−D are isoelectronic and have identical nuclei positions, the difference in calculated energies between B and C reflects the energy of interaction of the ligand electrons with the active site electric field, while the difference between structures C and D reflects the electronic strain energy.

For a ligand molecule in a fixed conformation, the optimal quantum chemical electronic distribution is calculated in an iterative fashion so that the electrons and nuclei are present in a SCF. This SCF is represented by structure D with the electronic energy of the ligand designated E_{lig} (eq 4).

$$E_D = E_{lig} \tag{4}$$

If this conformation of the ligand with its associated electronic distribution were placed in the electric field generated by an enzyme active site, an electronic energy of the unperturbed system could be determined from the sum of E_{lig} and the electrostatic interactions of the electrons and nucleus with the active site electric field, given by E_{El}. In addition, the electrons are free to move, i.e., to become polarized in response to the electric field. This polarization must lead to an increase in the electronic energy of the molecule considered in isolation, ΔE_{lig}, but is more than offset by a favorable change in the electrostatic interaction energy, ΔE_{El}; i.e., $\Delta E_{lig} + \Delta E_{El}$ must be negative. Thus, the electronic energy of the complex in Scheme 2B is given by eq 5.

$$E_B = E_{lig} + E_{El} + \Delta E_{lig} + \Delta E_{El} \tag{5}$$

As suggested by eq 6, this polarization will occur as long as the increase in ΔE_{lig} is smaller in magnitude than the decrease in ΔE_{El}.

[4] Conceptually, it would have been preferable to use the electron density for the substrate obtained from the ONIOM calculation directly, but because there is a small amount of charge transfer, it is impossible to identify the electrons from the substrate. This problem is solved when all of the electrons must be associated with the substrate as is the case when the protein is modeled as partial charges.

$$\partial(E_B)/\partial(e^- \text{ polarization}) = \partial(\Delta E_{lig})/\partial(e^- \text{ polarization}) + \partial(\Delta E_{El})/\partial(e^- \text{ polarization}) \quad (6)$$

$$E_C = E_{lig} + \Delta E_{lig} \quad (7)$$

In a theoretical experiment, the active site electric field may be removed while retaining the polarization of the electrons, i.e., to go from B to C in Scheme 2. In this thought process, the electrostatic interaction terms are lost while the cost of the electronic polarization is retained. Thus, E_C is given as the sum of the SCF energy of the ligand and the energetic cost of polarizing the ligand electrons. Computationally, as shown in eq 8, this energetic cost is determined as the difference in energies for structures B and C.

$$\Delta E_{lig} = E_B - E_C \quad (8)$$

For the binding of DAC-CoA to the active site of ECH, the quantum chemical calculation indicates that ΔE_{lig} is 3.2 kcal/mol. Any dissection of an overall binding energy into component parts becomes a matter of definition. Our definition of electronic strain energy based on Scheme 2 is a very restrictive definition. All of the constraints placed on the calculation have minimized the calculated electronic strain; in particular, two major contributions that would increase the calculated electronic strain have been omitted. Charge transfer contributions, such as those that lead to partial covalent character in H-bonds, are neglected since the calculation represented the H-bond partners as partial charges and not nuclei. Additionally, the restriction of the bond lengths and angles in the relaxation from B to C in Scheme 2 reduces the calculated electronic strain by limiting the extent of polarization that is possible. However, this effect is anticipated to be small since one of the qualitative results of previous model studies of polarization of enoyl thiolesters by uniform electric fields is that electronic redistribution of the magnitude observed in these calculations results in bond length changes of $\leq$0.02 Å (*58*).

While the calculated electronic strain is only ~25% of the 13 kcal/mol of potential ground electronic state destabilization determined by UV spectroscopy, it could play a significant role in the catalytic power of the enzyme. If, as suggested by Scheme 1, this substrate activation reduces the activation energy by 3.2 kcal/mol, it results in an ~200-fold increase in the rate constant for hydration of the carbon−carbon double bond. The interpretation that the 3.2 kcal/mol decreases the activation energy relies on the similarity of the electronic polarization we have observed in the ground state and the presumed enol(ate) transition state that has been ascribed to the reactions catalyzed by the enoyl-CoA hydratase/isomerase superfamily (*20*, *59*−*64*). Experimentally, the effect of the induction of positive charge at the electrophilic β-carbon has been shown to enhance the rate of reaction as the addition of thiophenoxide to a series of para-substituted β-chloro-β-phenylcinnamic acid methyl esters varied the rate more than 40-fold (*65*).

SUMMARY

The experimental changes in ^{13}C NMR shielding of the carbonyl, α-, and β-carbons have been reproduced by a GIAO calculation for DAC-CoA based on the crystal structure of the active site determined in the preceding paper. The qualitative agreement between experiment and theory permits the calculated quantum chemical electronic distributions and associated energies to be used to provide an estimate of the electronic rearrangement required to generate the observed change in spectroscopic properties and to provide a strict definition of electronic strain energy. For ECH, the calculated electronic strain energy of 3.2 kcal/mol suggests that electronic strain plays a modest role in enhancing the rate constant for nucleophilic addition to the β-carbon.

ACKNOWLEDGMENT

The NMR spectra were acquired with the assistance of Jim van Epp at the Brown Chemistry Department NMR facility (NIH RR). Computational support was provided by the Ohio Supercomputer Center.

REFERENCES

1. Bayliss, W. M. (1925) *The Nature of Enzyme Action*, 5th ed., Longmans, Green & Co., London.
2. Eyring, H., Lumry, R., and Spikes, J. D. (1954) in *The Mechanism of Enzyme Action* (McElroy, W. D., and Glass, B., Eds.) pp 123−140, Johns Hopkins Press, Baltimore.
3. Quastel, J. H. (1926) *Biochem. J. 20*, 166.
4. Wolfenden, R. (1976) *Annu. Rev. Biophys. Bioeng. 5*, 270−306.
5. Pauling, L. (1948) *Nature 161*, 707−710.
6. Warshel, A., and Weiss, R. M. (1981) *Ann. N.Y. Acad. Sci. 367*, 370−382.
7. Warshel, A., Aqvist, J., and Creighton, S. (1989) *Proc. Natl. Acad. Sci. U.S.A. 86*, 5820−5824.
8. Warshel, A. (2000) *Theor. Chem. Acc. 103*, 337−339.
9. Schramm, V. L. (1998) *Annu. Rev. Biochem. 67*, 693−720.
10. Müller-Newen, G., Janssen, U., and Stoffel, W. (1995) *Eur. J. Biochem. 228*, 68−73.
11. Engel, C. K., Mathieu, M., Zeelen, J. P., Hiltunen, J. K., and Wierenga, R. K. (1996) *EMBO J. 15*, 5135−5145.
12. Engel, C. K., Kiema, T. R., Hiltunen, J. K., and Wierenga, R. K. (1998) *J. Mol. Biol. 275*, 847−859.
13. Benning, M. M., Haller, T., Gerlt, J. A., and Holden, H. M. (2000) *Biochemistry 39*, 4630−4639.
14. Bell, A. F., Wu, J., Feng, Y., and Tonge, P. J. (2001) *Biochemistry 40*, 1725−1733.
15. D'Ordine, R. L., Tonge, P. J., Carey, P. R., and Anderson, V. E. (1994) *Biochemistry 33*, 12635−12643.
16. Taylor, K., Liu, R., Liang, P., Price, J., Dunaway-Mariano, D., Tonge, P., Clarkson, J., and Carey, P. (1995) *Biochemistry 34*, 13881−13888.
17. Clarkson, J., Tonge, P. J., Taylor, K. L., Dunaway-Mariano, D., and Carey, P. R. (1997) *Biochemistry 36*, 10192−10199.
18. Taylor, K. L., Xiang, H., Liu, R. Q., Yang, G., and Dunaway-Mariano, D. (1997) *Biochemistry 36*, 1349−1361.
19. Steinman, H. M., and Hill, R. L. (1975) *Methods Enzymol. 35*, 136−151.
20. Bahnson, B. J., and Anderson, V. E. (1991) *Biochemistry 30*, 5894−5906.
21. Meyers, A. I., Spohn, R. F., and Linderman, R. J. (1985) *J. Org. Chem. 50*, 3633−3635.
22. Kawaguchi, A., Yoshimura, T., and Okuda, S. (1981) *J. Biochem. 89*, 337−339.
23. Tonge, P. J., Anderson, V. E., Fausto, R., Kim, M., M., P.-C., and R., C. P. (1995) *J. Biol. Spectrosc. 1*, 387−394.
24. Hoye, T. R., Martin, S. J., and Peck, D. R. (1982) *J. Org. Chem. 47*, 331.
25. Ronald, R. C. (1975) *Tetrahedron Lett.*, 3973.
26. Pratt, E. F., and Van De Castle, J. F. (1961) *J. Org. Chem. 26*, 2973.
27. Still, W. C., Khan, M., and Mitra, A. (1978) *J. Org. Chem. 43*, 2923−2925.

28. Lee, C. H., and Sarma, R. H. (1975) *J. Am. Chem. Soc. 97*, 1225−1236.
29. Jaffe, E. K., and Markham, G. D. (1987) *Biochemistry 26*, 4258−4264.
30. de Dios, A. C., and Oldfield, E. (1993) *Chem. Phys. Lett. 205*, 108−116.
31. de Dios, A. C., Pearson, J. G., and Oldfield, E. (1993) *Science 260*, 1491−1496.
32. Karadakov, P. B., and Morokuma, K. (2000) *Chem. Phys. Lett. 317*, 589−596.
33. Sternberg, U., and Priess, W. (1997) *J. Magn. Reson. 125*, 8−19.
34. Ditchfield, R. (1974) *Mol. Phys. 27*, 789.
35. Wolinski, K., Hilton, J. F., and Pulay, P. (1990) *J. Am. Chem. Soc. 112*, 8251.
36. Dapprich, S., Komaromi, I., Byun, K. S., Morokuma, K., and Frisch, M. J. (1999) *THEOCHEM 462*, 1−21.
37. Frisch, M. J., Trucks, G. W., Schlegel, H. B., Scuseria, G. E., Robb, M. A., Cheeseman, J. R., Zakrzewski, V. G., Montgomery, J. A., Jr., Stratmann, R. E., Burant, J. C., Dapprich, S., Millam, J. M., Daniels, A. D., Kudin, K. N., Strain, M. C., Farkas, O., Tomasi, J., Barone, V., Cossi, M., Cammi, R., Mennucci, B., Pomelli, C., Adamo, C., Clifford, S., Ochterski, J., Petersson, G. A., Ayala, P. Y., Cui, Q., Morokuma, K., Malick, D. K., Rabuck, A. D., Raghavachari, K., Foresman, J. B., Cioslowski, J., Ortiz, J. V., Stefanov, B. B., Liu, G., Liashenko, A., Piskorz, P., Komaromi, I., Gomperts, R., Martin, R. L., Fox, D. J., Keith, T., Al-Laham, M. A., Peng, C. Y., Nanayakkara, A., Gonzalez, C., Challacombe, M., Gill, P. M. W., Johnson, B., Chen, W., Wong, M. W., Andres, J. L., Gonzalez, C., Head-Gordon, M., Replogle, E. S., and Pople, J. A. (1998) *Gaussian 98*, version A.3, Gaussian Inc., Pittsburgh, PA.
38. Becke, A. D. (1993) *J. Chem. Phys. 98*, 5648.
39. Honig, B., and Nicholls, A. (1995) *Science 268*, 1144−1149.
40. Cornell, W., Cieplak, P., Bayly, C., Gould, I., Merz, K., Ferguson, D., Spellmeyer, D., Fox, T., Caldwell, J., and Kollman, P. (1995) *J. Am. Chem. Soc. 117*, 5179−5197.
41. Bergman, D. L., Laaksonen, L., and Laaksonen, A. (1997) *J. Mol. Graphics Modell. 15*, 301−306.
42. Laaksonen, L. (1992) *J. Mol. Graphics 10*, 33−34.
43. Laaksonen, L. (2001) *gOpenmol*, version 2.0, Espoo, Finland.
44. Hass, G. M., and Hill, R. L. (1969) *J. Biol. Chem. 244*, 6080−6086.
45. Minami-Ishii, N., Taketani, S., Osumi, T., and Hashimoto, T. (1989) *Eur. J. Biochem. 185*, 73−78.
46. Allerhand, A. (1978) *Methods Enzymol. 61*, 458−549.
47. Kurz, L. C., and Frieden, C. (1987) *Biochemistry 26*, 8450−8457.
48. Sanders, J. K., and Hunter, B. K. (1987) in *Modern NMR Spectroscopy: A Guide for Chemists*, Chapter 7, Oxford University Press, New York.
49. Speisecke, H., and Schneider, W. G. (1961) *Tetrahedron Lett.*, 468−472.
50. Lantz, M. H. (2000) Ph.D. Thesis, Case Western Reserve University, Cleveland, OH.
51. Pearson, J. G., Le, H. B., Sanders, L. K., Godbout, N., Havlin, R. H., and Oldfield, E. (1997) *J. Am. Chem. Soc. 119*, 11941−11950.
52. Oldfield, E. (1995) *J. Biomol. NMR 5*, 217−225.
53. Altose, M. D., Zheng, Y., Dong, J., Palfey, B. A., and Carey, P. R. (2001) *Proc. Natl. Acad. Sci. U.S.A. 98*, 3006−3011.
54. Wu, W. J., Anderson, V. E., Raleigh, D. P., and Tonge, P. J. (1997) *Biochemistry 36*, 2211−2220.
55. Bahnson, B. J., Anderson, V. E., and Petsko, G. A. (2002) *Biochemistry 41*, 2621−2629.
56. Anderson, V. E. (1999) in *Encyclopedia of Molecular Biology* (Creighton, T. E., Ed.) John Wiley, New York.
57. Fausto, R., Tonge, P. J., and Carey, P. R. (1994) *J. Chem. Soc., Faraday Trans. 90*, 3491−3503.
58. Anderson, V. E. (1999) in *Proceedings of the 36th Steenbock Symposium on Enzyme Mechanisms*, pp 85−97, IOS Press, Amsterdam.
59. Gerlt, J. A., and Gassman, P. G. (1993) *J. Am. Chem. Soc. 115*, 11552−11568.
60. Gerlt, J. A., and Babbitt, P. C. (1998) *Curr. Opin. Chem. Biol. 2*, 607−612.
61. Holden, H. M., Benning, M. M., Haller, T., and Gerlt, J. A. (2001) *Acc. Chem. Res. 34*, 145−157.
62. Anderson, S. R., Anderson, V. E., and Knowles, J. R. (1994) *Biochemistry 33*, 10545−10555.
63. Hofstein, H. A., Feng, Y., Anderson, V. E., and Tonge, P. (1999) *Biochemistry 38*, 9508−9516.
64. Bahnson, B. J., and Anderson, V. E. (1989) *Biochemistry 28*, 4173−4181.
65. Youssef, A.-H. A., Sharaf, S. M., El-Sadany, S. K., and Hamed, E. A. (1981) *J. Org. Chem. 46*, 3813−3816.
66. Bergman, D. L., Laaksonen, L., and Laaksonen, A. (1997) *J. Mol. Graphics Modell. 15*, 328−333.
67. Dakoji, S., Li, D., Agnihotri, G., Zhou, H. Q., and Liu, H. W. (2001) *J. Am. Chem. Soc. 123* (40), 9749−9759.

BI015845H